Multi-omic analysis of lung tumors defines pathways activated in neuroendocrine transformation

Alvaro Quintanal-Villalonga[1*], Hirokazu Taniguchi[1], Yingqian A. Zhan[2], Maysun M. Hasan[3], Shweta S. Chavan[4], Fanli Meng[3], Fathema Uddin[1], Parvathy Manoj[1], Mark T.A. Donoghue[4], Helen H. Won[4], Joseph M. Chan[1,5,6], Metamia Ciampricotti[1], Andrew Chow[1], Michael Offin[1], Jason C. Chang[7], Jordana Ray-Kirton[8], Sam E. Tischfield[3], Jacklynn Egger[1], Umesh K. Bhanot[8], Irina Linkov[8], Marina Asher[8], Sonali Sinha[8], Joachim Silber[7,8], Christine A. Iacobuzio-Donahue[7,9,10], Michael H. Roehrl[7,8,10], Travis J. Hollmann[7,10], Helena A. Yu[1,11], Juan Qiu[12], Elisa de Stanchina[12], Marina K. Baine[7], Natasha Rekhtman[7], John T. Poirier[13], Brian Houck-Loomis[4], Richard P. Koche[2], Charles M. Rudin[1,11*]. Triparna Sen[1,11, * #].

1. Department of Medicine, Thoracic Oncology Service, Memorial Sloan Kettering Cancer Center, New York, NY, USA.
2. Center for Epigenetics Research, Memorial Sloan Kettering Cancer Center, New York, NY 10065, USA.
3. Sloan Kettering Institute, Memorial Sloan Kettering Cancer Center, New York, NY.
4. Marie-Josée and Henry R. Kravis Center for Molecular Oncology, Memorial Sloan Kettering Cancer Center, New York, NY.
5. Program for Computational and Systems Biology, Sloan Kettering Institute, Memorial Sloan Kettering Cancer Center, New York, NY, USA.
6. Parker Institute for Cancer Immunotherapy, Memorial Sloan Kettering Cancer Center, New York, NY, USA.
7. Department of Pathology, Memorial Sloan Kettering Cancer Center, New York, New York.
8. Precision Pathology Center, Memorial Sloan Kettering Cancer Center, New York, New York.
9. David M. Rubenstein Center for Pancreatic Cancer Research, Memorial Sloan Kettering Cancer Center, New York, NY, USA.
10. Human Oncology and Pathogenesis Program, Memorial Sloan Kettering Cancer Center, New York, New York.
11. Weill Cornell Medical College, New York, New York.
12. Antitumor Assessment Core, Memorial Sloan Kettering Cancer Center, New York, NY 10065, USA.
13. Perlmutter Cancer Center, New York University Langone Health, New York, New York.

*Co-corresponding authors: quintaa1@mskcc.org (AQV), rudinc@mkcc.org (CMR) and sent@mskcc.org (TS)

Lead Contact: sent@mskcc.org (TS);

Running title: Multi-omic analysis of neuroendocrine transformation

SUPPLEMENTARY TABLE LEGENDS

Supplementary Table S1. Summary of clinical characteristics of the cohorts under study

Supplementary Table S2. Clinical information of the transformation cohort

Supplementary Table S3. Clinical information of the control LUAD cohort

Supplementary Table S4. Clinical information of the control SCLC cohort

Supplementary Table S5. Exonic mutations on cancer genes from WES

Supplementary Table S6. Focal Copy Number Alterations on Cancer Genes

Supplementary Table S7. Enrichment of mutations and CNAs in the T-LUAD cohort versus TCGA cohort

Supplementary Table S8. Arm level copy number stats for cases included in the genomic evolution analyses

Supplementary Table S9. SCLC subtype determining TF expression in samples in our cohorts

Supplementary Table S10. RNAseq gene expression levels per sample.

Supplementary Table S11. Applications per sample

Supplementary Table S12. Quantification of the phospho-kinase array

Supplementary Table S13. WES quality control

Supplementary Table S14. Methylation (EPIC) data quality control

Supplementary Table S15. RNAseq data quality control

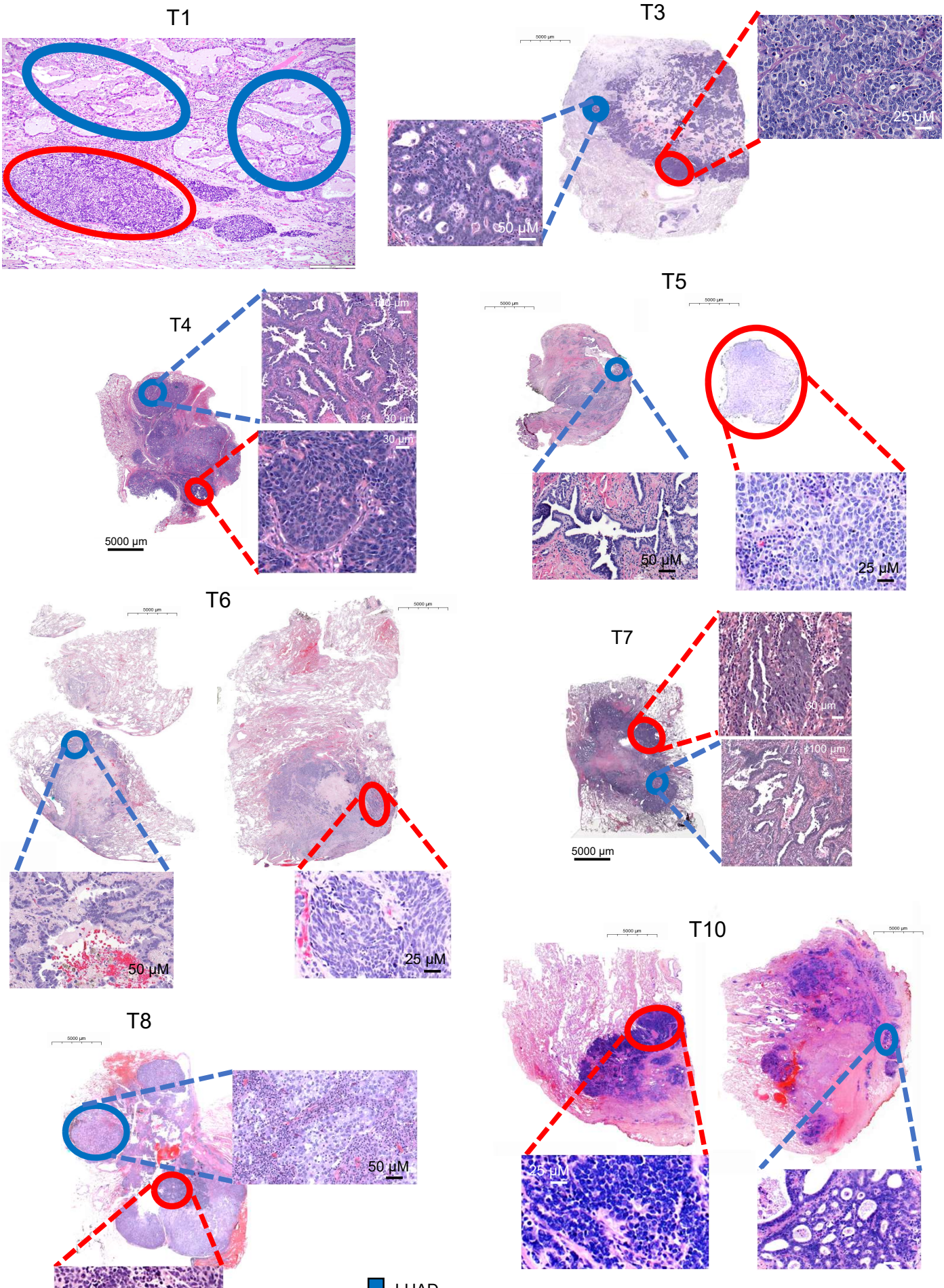

Supplementary Figure S1

Supplementary Figure S1. H&E staining of the combined LUAD/SCLC cases in our cohort with histologic components labeled.

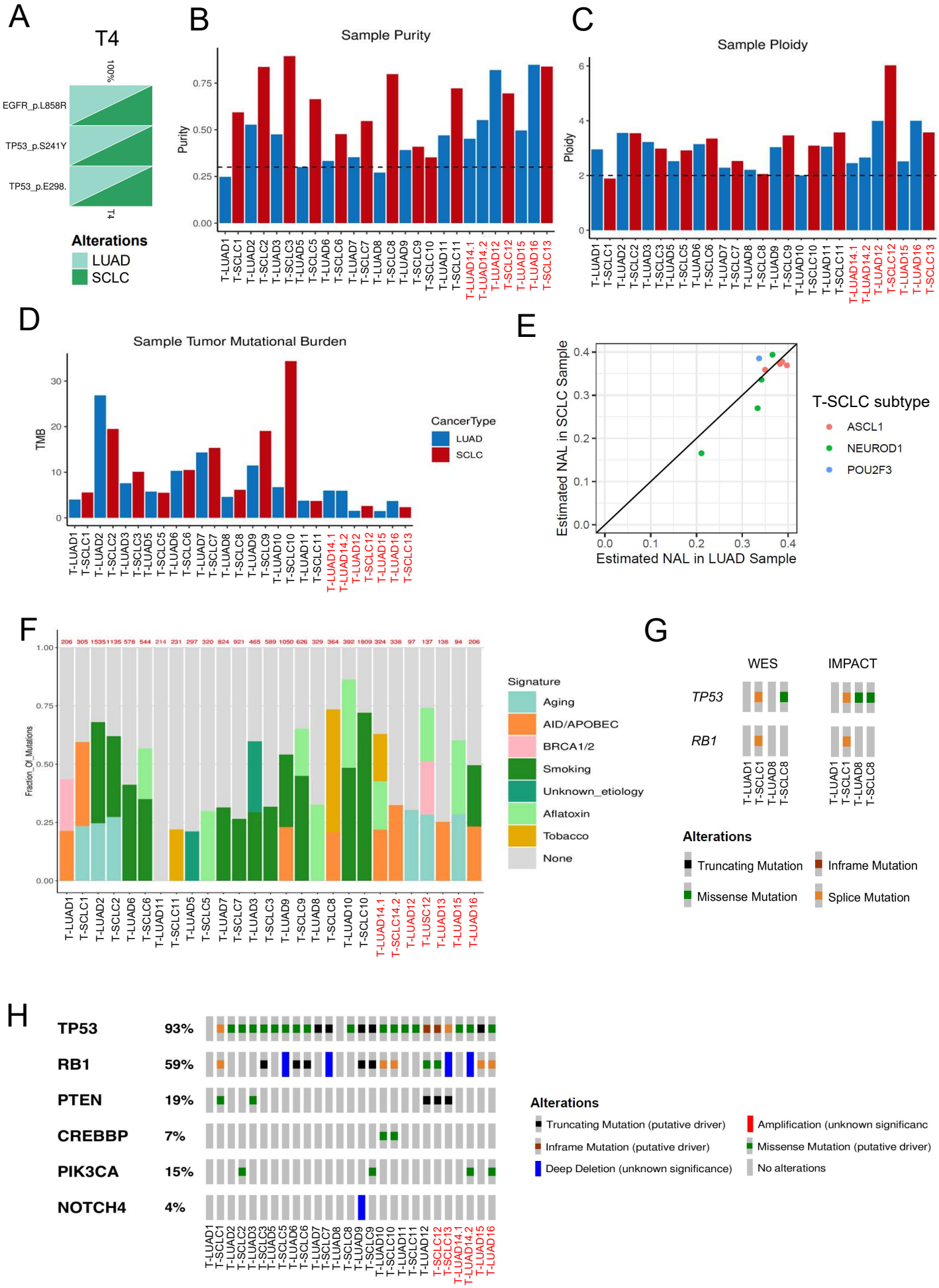

Supplementary Figure S2

Supplementary Figure S2. (A) Common mutations in the LUAD and SCLC components of the T4 case, assessed in the RNAseq data. Bar plots showing tumor purity (B), ploidy (C) and mutational burden (D) of samples in the cohort analyzed by WES. (E) Neoantigen load in matched T-LUAD and T-SCLC samples labeled by subtype of the SCLC component. (F) Enrichment in mutational signatures on the samples in our cohort analyzed by WES. (G) Oncoprint showing discrepancies in SNVs for cases T1 and T8 between WES and targeted sequencing. *RB1* and *TP53* private mutations in T-SCLC1 by WES are truly private as confirmed by IMPACT targeted deep sequencing. *TP53* private mutation in T-SCLC8 by WES was called in IMPACT at a low VAF (VAF=0.06) in T-LUAD8. Therefore, this mutation is not truly private. Upon genotyping in WES we could find read evidence at a subclonal level (VAF<5%) given lower depth of sequencing in WES. (H) Oncoprint of mutations frequently found in T-SCLC(70) in our samples analyzed by WES. Samples IDs in black and red indicate that they come from a combined histology specimen or a pre-/post-transformation specimen, respectively.

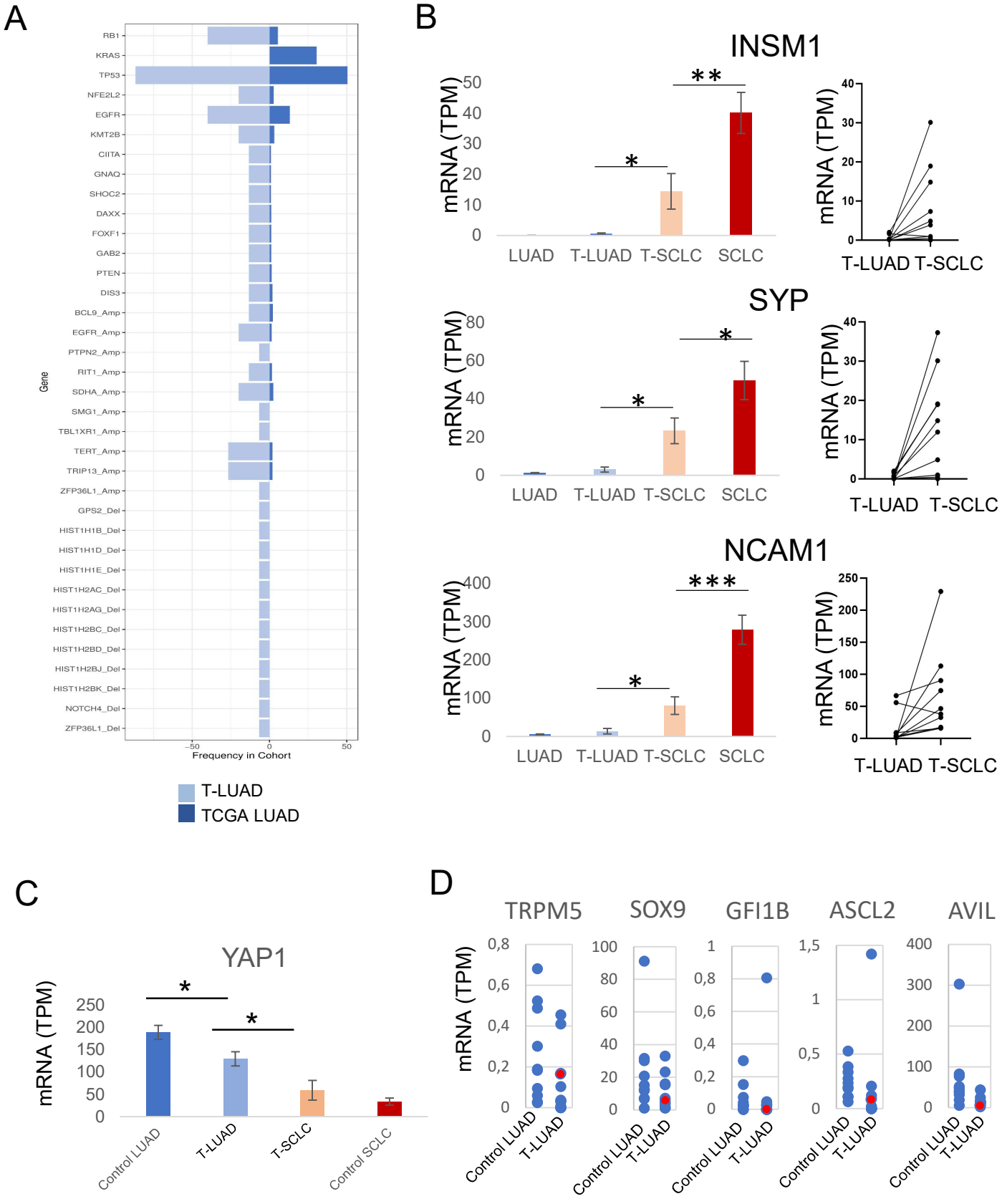

Supplementary Figure S3

Supplementary Figure S3. (A) Prevalence (%) of mutations and CNAs enriched in our cohort of T-LUADs versus TCGA LUAD cohort (p-value<0.05). (B) mRNA expression of canonical NE markers in the different categories of samples included in our cohort. (C) YAP1 mRNA expression in control LUAD, T-LUAD, T-SCLC, and *de novo* SCLC samples. Two tailed Student's t-test was used to assess statistical significance of the differential expression between groups (D) mRNA expression of tuft cell markers(20) in our control and T-LUADs. The expression values for the LUAD component of T3 are highlighted in red. Two tailed Student's t-test was used to assess statistical significance of the differential expression between groups. p-values legend: * p<0.05, ** p<0.01, *** p<0.001. Samples IDs in black and red indicate that they come from a combined histology specimen or a pre-/post-transformation specimen, respectively.

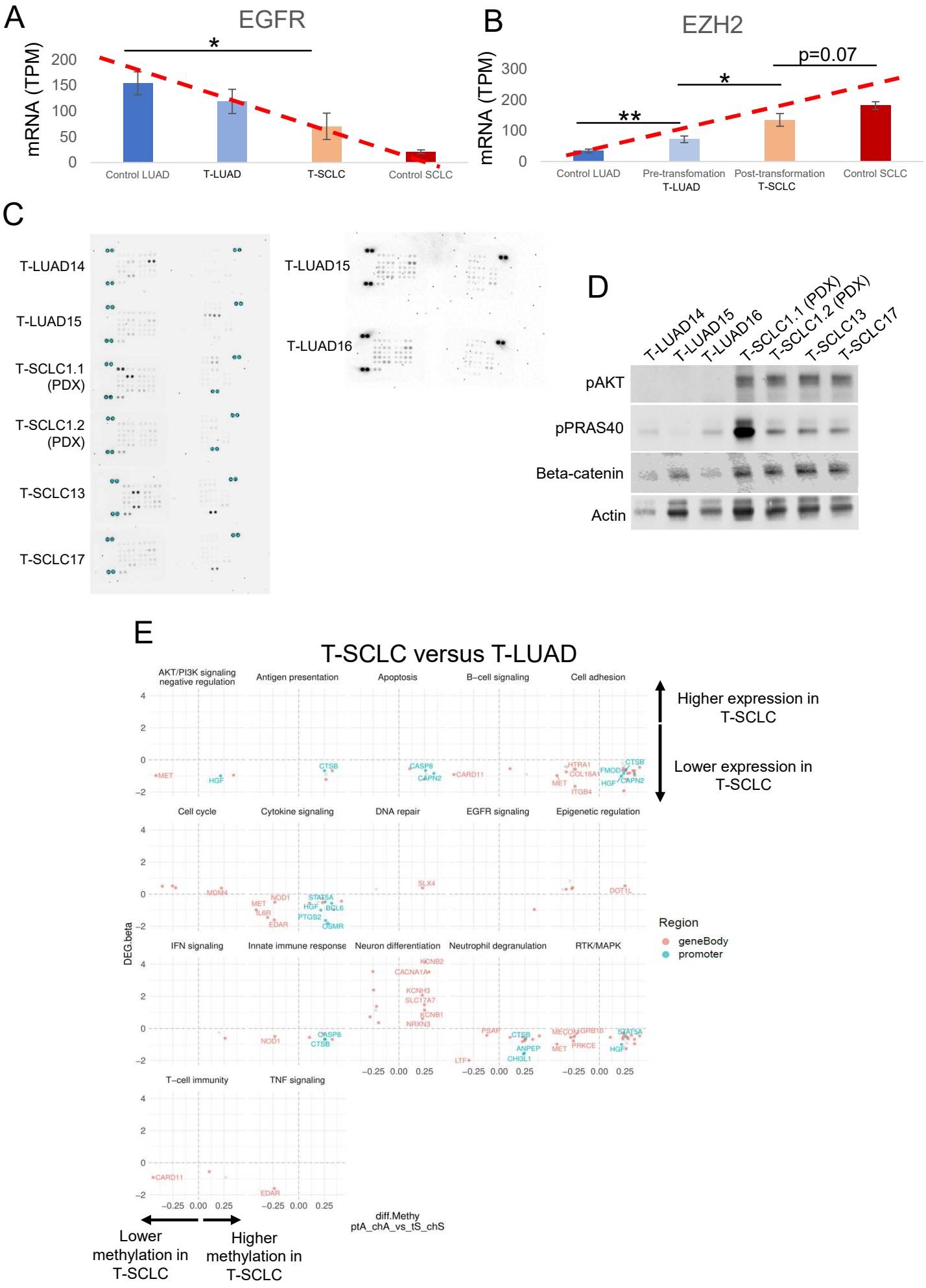

Supplementary Figure S4

Supplementary Figure S4. *EZH2* (A) and *EGFR* (B) mRNA expression in control LUAD, T-LUAD, T-SCLC, and *de novo* SCLC samples. Two tailed Student's t-test was used to assess statistical significance of the differential expression between groups. (C) Blots for the protein arrays performed in this study. (D) Western blot showing levels of pAKT, pPRAS40 and beta-catenin in the protein samples included in the protein arrays. (E) Scatter plots showing DEGs exhibiting differential methylation levels in T-LUAD vs. T-SCLC, grouped by pathways found enriched or depleted in our pathway enrichment analyses on RNA data. For DEGs, beta value (Sleuth-based estimation of log2 fold change) is shown. Significantly differentially expressed (q value < 0.05 and beta >= log2(1.5)) and methylated (FDR < 0.5 and differential methylation level greater than 0.1) sites are highlighted. Those genes where increased gene body or promoter methylation is correlated to expression positively and negatively, respectively, are labeled. p-values legend: * $p<0.05$, ** $p<0.01$.

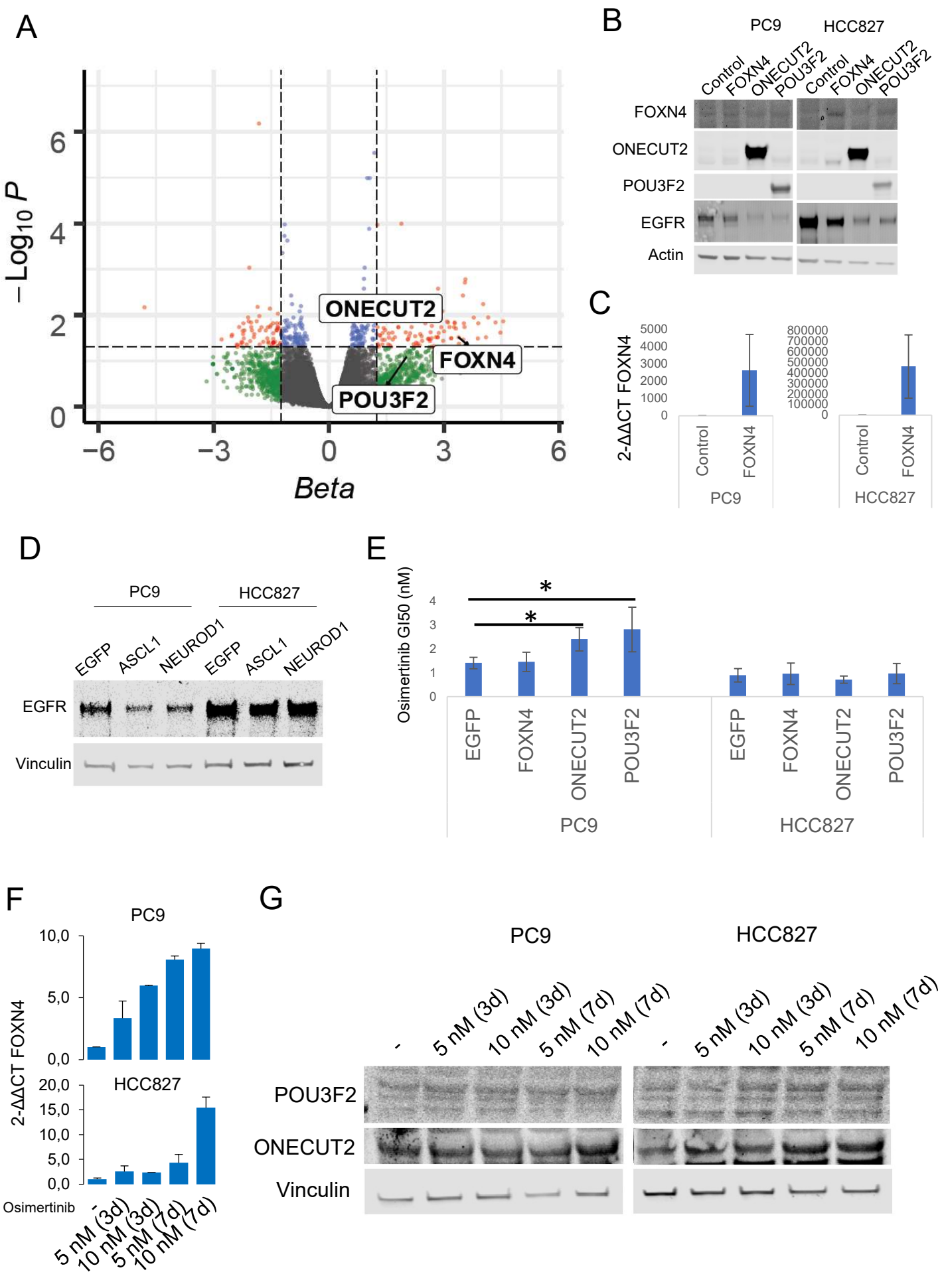

Supplementary Figure S5

Supplementary Figure S5. (A) Volcano plot showing overexpression of transcription factors of interest at the RNA level in T-SCLC versus T-LUAD. For DEGs, beta value (Sleuth-based estimation of log2 fold change) is shown. (B) Western blots exhibiting downregulation of EGFR after overexpression of FOXN4, ONECUT2 or POU3F2 in two *EGFR*-mutant lung LUAD cell lines. (C) Confirmation of FOXN4 overexpression at the RNA level by qPCR. (D) Western blots showing EGFR expression levels after ASCL1 and NEUROD1 overexpression in these cell lines. (E) Osimertinib concentrations inducing 50% of growth inhibition (GI50) in these cell lines overexpressing FOXN4, ONECUT2 or POU3F2 GI50 were calculated as described in(69,71). FOXN4 mRNA (F) and ONECUT2 or POU3F2 protein (G) levels after treatment with Osimertinib 5 nM or 10 nM for 3 or 7 days. Representative biological replicates are shown for qPCR and western blots. Two tailed Student's t-test was used to assess statistical significance of the differential Osimertinib sensitivity between cell lines. p-value legend: * $p<0.05$

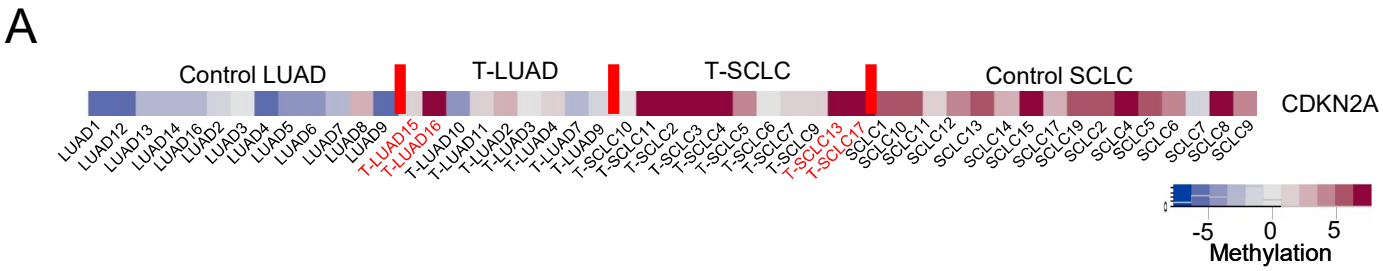

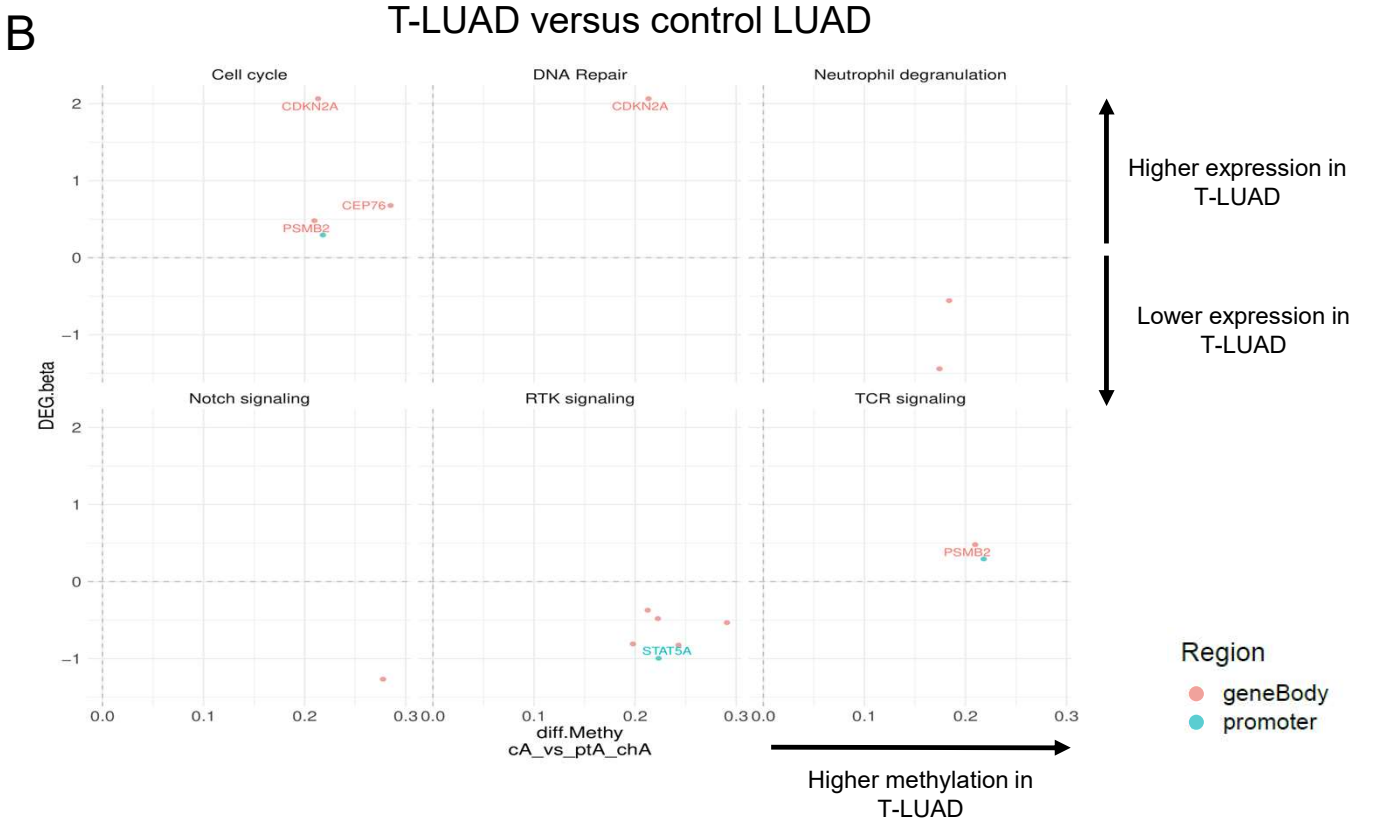

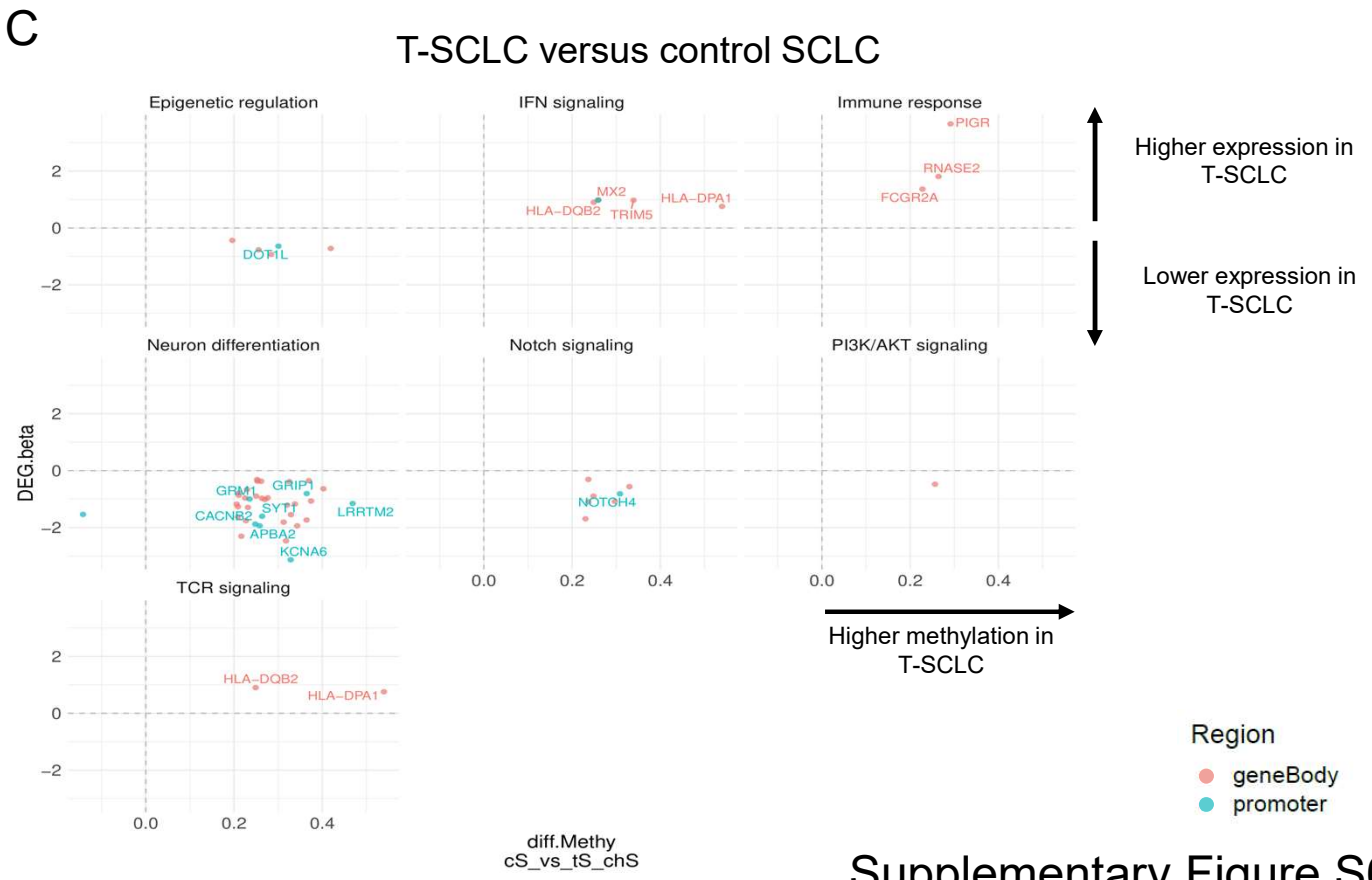

Supplementary Figure S6

Supplementary Figure S6. (A) *CDKN2A* body methylation levels in the samples in our cohort analyzed by EPIC. Scatter plots showing DEGs exhibiting differential methylation levels in our T-LUAD versus control LUAD (B) or T-SCLC versus *de novo* SCLC (C) comparisons, grouped by pathways enriched or depleted in pathway enrichment analyses on RNA. For DEGs, beta value (Sleuth-based estimation of log2 fold change) is shown. Significantly differentially expressed (q value < 0.05 and beta >= log2(1.5)) and methylated (FDR < 0.5 and differential methylation level greater than 0.1) sites are highlighted. Those genes where increased gene body or promoter methylation is correlated to expression positively and negatively, respectively, are labeled. Samples IDs in black and red indicate that they come from a combined histology specimen or a pre-/post-transformation specimen, respectively.

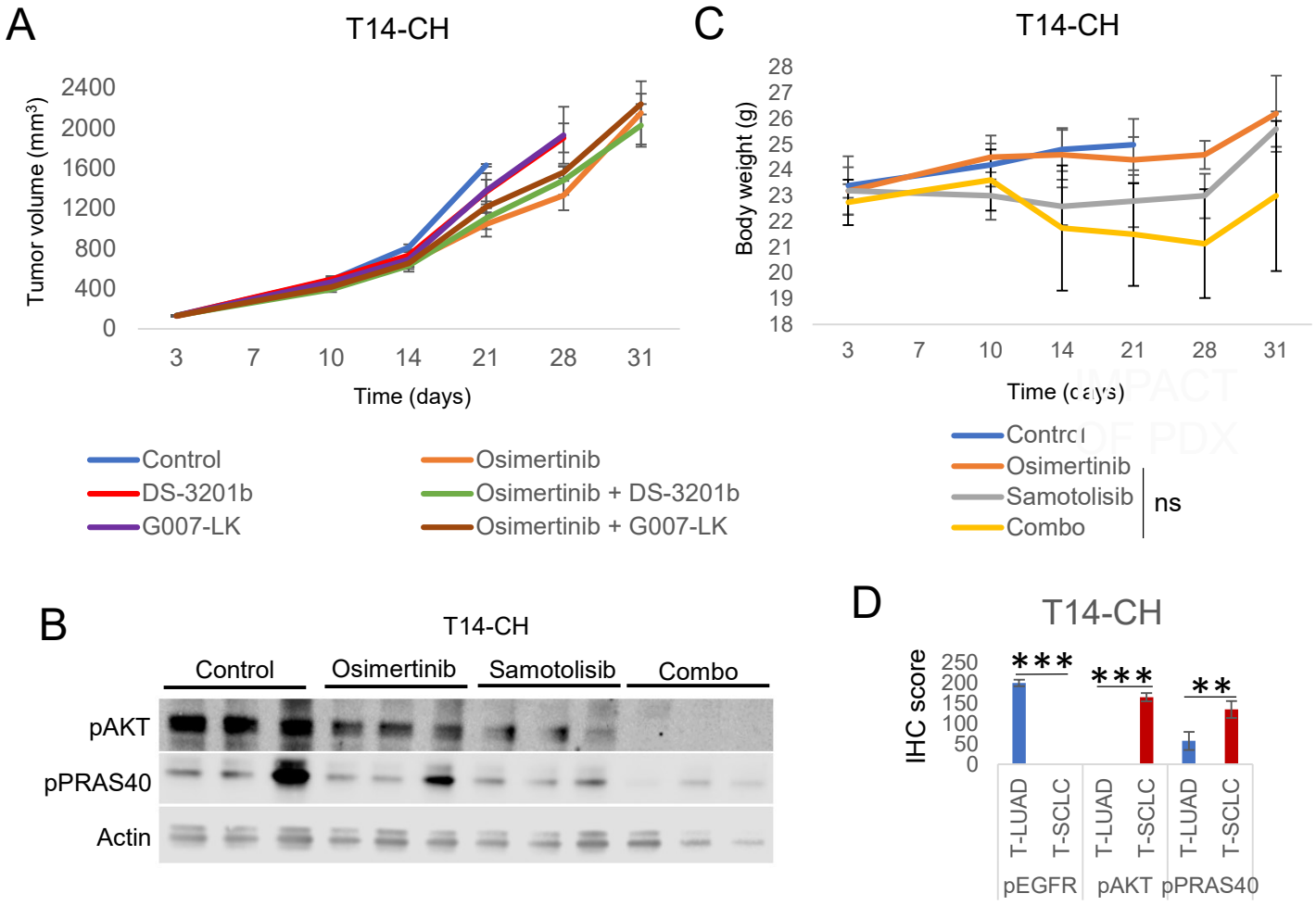

Supplementary Figure S7

Supplementary Figure S7. (A) Tumor volume measurements for the treatment of the T14-CH *EGFR*-mutant combined LUAD and NE PDX model with the EGFR inhibitor Osimertinib, the EZH1/2 inhibitor DS-3201b, an the Wnt inhibitor G007-LK, or the combinations of Osimertinib with the two latter. (B) Western blot showing AKT and PRAS40 phosphorylation levels in T14-CH PDX tumors (N=3 per arm) treated with osimertibib, samotolisib, or their combination. (C) Body weight measurements of the mice treated with Osimertinib, the AKT inhibitor Somatolisib, or their combination (see **Figure 7A**). Two-tailed Student's t-test was performed to compare body weights at endpoint (day 31). (D) Plot showing average ± SD of IHC scores for pEGFR, pAKT and pPRAS40 in the LUAD and SCLC components of control T14-CH, Two-tailed Student's t-test was performed to compare IHC scores between histological components . p-values legend: * $p<0.05$, ** $p<0.01$, *** $p<0.001$, ns = Non-significant.